PNAS RESEARCH ARTICLE | CELL BIOLOGY

Harnessing endogenous transcription factors directly by small molecules for chemically induced pluripotency inception

Yan Jin[a,1], Yunkun Lu[a,1], Lianyu Lin[a], Chao Liu[b,c], Xiaojie Ma[a], Xi Chen[a], Ziyu Zhou[a], Zhensheng Hu[a], Jiaqi Pu[a,d], Guo Chen[a], Qian Deng[a], Liling Jiang[a], Yuhan Li[a], Yulong Zhao[b,c], Hao Wang[e], Junfen Fu[d], Wei Li[b,c], and Saiyong Zhu[a,2]

Edited by Janet Rossant, Gairdner Foundation, Toronto, Canada; received September 5, 2022; accepted March 27, 2023

Chemistry-alone approach has recently been applied for incepting pluripotency in somatic cells, representing a breakthrough in biology. However, chemical reprogramming is hampered by low efficiency, and the underlying molecular mechanisms remain unclear. Particularly, chemical compounds do not have specific DNA-recognition domains or transcription regulatory domains, and then how do small molecules work as a driving force for reinstating pluripotency in somatic cells? Furthermore, how to efficiently clear materials and structures of an old cell to prepare the rebuilding of a new one? Here, we show that small molecule CD3254 activates endogenous existing transcription factor RXRα to significantly promote mouse chemical reprogramming. Mechanistically, CD3254–RXRα axis can directly activate all the 11 RNA exosome component genes (*Exosc1–10* and *Dis3*) at transcriptional level. Unexpectedly, rather than degrading mRNAs as its substrates, RNA exosome mainly modulates the degradation of transposable element (TE)-associated RNAs, particularly *MMVL30*, which is identified as a new barrier for cell-fate determination. In turn, *MMVL30*-mediated inflammation (IFN-γ and TNF-α pathways) is reduced, contributing to the promotion of successful reprogramming. Collectively, our study provides conceptual advances for translating environmental cues into pluripotency inception, particularly, identifies that CD3254–RXRα–RNA exosome axis can promote chemical reprogramming, and suggests modulation of TE-mediated inflammation via CD3254-inducible RNA exosome as important opportunities for controlling cell fates and regenerative medicine.

chemical reprogramming | CD3254 | RXRα | RNA exosome | transposable elements

Cellular reprogramming has fascinated the scientific community and general public for decades (1). Advances in the field provide essential approaches for regenerative medicine (2). Transcription factors (TFs) are a natural choice for reprogramming, but exogenous TFs have to be delivered into starting cells, which is labor intensive and raises potential safety concerns. Chemical compounds not only are more convenient and nonintegrating for manipulating cell fates, but also can provide a better understanding of cell-fate transitions (3, 4). Unfortunately, chemical reprogramming remains a slow and inefficient process, hindering its broad applications (5–11). Then, more efforts are required to identify new small molecules for rapid and efficient chemical reprogramming. Besides technical innovations and advances, many efforts were also made to elucidate the molecular mechanisms of cellular reprogramming. Several important cellular and molecular mechanisms have been identified as hallmarks of pluripotent reprogramming, including epigenetic regulation, mesenchymal-to-epithelial transition, and metabolic rewiring (12–17). So far, chemical reprogramming is still in its infancy, and the molecular understanding is very limited. There are many interesting questions in this research area: for example, how small molecules silence somatic genes, activate endogenous pluripotent gene regulatory network, and finally enable successful cell-fate transitions?

Nuclear receptors are interesting and special groups of transcription factors that can directly translate chemical signals into distinct physiologic effects and play important roles in development and physiology (18). Retinoid X receptor (RXR) can heterodimerize with other nuclear receptors, such as RAR and PPAR, and control multiple intertwined signaling pathways. RXR signaling pathway plays essential roles in development and has been harnessed for blood, brown fat, and pancreatic differentiation (4, 19–21). In addition, RXR signaling has been identified to be involved in tissue repair and regeneration (22). However, the precise molecular mechanisms are not completely understood. With the advent of new technologies, including RNA-Seq and cleavage under targets and tagmentation (CUT&Tag) (23), now we have the power to comprehensively dissect the direct downstream target genes of RXR, providing better understanding of nuclear receptor-mediated cellular functions. Particularly, starting from agonist–nuclear receptor axis can provide us a unique opportunity to dissect the

Significance

Chemistry-alone approach of converting one cell type into another has recently been demonstrated, representing a breakthrough in biology. However, chemical reprogramming is hampered by low efficiency, and the underlying molecular mechanisms remain unclear. Here, we study the key question of how do small molecules work as a driving force for reinstating pluripotency in somatic cells. We show that small molecule CD3254 activates endogenous transcription factor RXRα to significantly promote chemical reprogramming. Mechanistically, CD3254–RXRα axis can directly activate all 11 RNA exosome component genes at transcriptional level. RNA exosome modulates the degradation of transposable element-associated RNAs and then inflammation is reduced, contributing to successful reprogramming. In summary, our study provides conceptual advances for cellular reprogramming and technical improvement for regenerative medicine.

Author contributions: Y.J. and S.Z. designed research; Y.J., Y. Lu, C.L., Y.Z., and W.L. performed research; X.M., X.C., Z.Z., Z.H., J.P., G.C., Q.D., L.J., Y. Li, H.W., and J.F. contributed new reagents/analytic tools; Y.J., Y. Lu, L.L., W.L., and S.Z. analyzed data; and Y.J., Y. Lu, and S.Z. wrote the paper.

The authors declare no competing interest.

This article is a PNAS Direct Submission.

[1]Y.J. and Y. Lu contributed equally to this work.

[2]To whom correspondence may be addressed. Email: saiyong@zju.edu.cn.

This article contains supporting information online at https://www.pnas.org/lookup/suppl/doi:10.1073/pnas.2215155120/-/DCSupplemental.

Published May 16, 2023.

fundamental questions about reinstating pluripotency in somatic cells by only environmental cues.

RNA surveillance ensures precise control of RNA homeostasis in a spatiotemporally controlled manner and safeguards normal development (24–28). RNA exosome, a multiprotein complex with 3′ to 5′ ribonuclease activity, including 11 subunits (Exosc1–10 and Dis3) in total, is a key component involved in RNA surveillance (29–32). Cell-fate transitions, with the accompanying rapid degradation and synthesis of a plethora of RNAs, present a challenge for precise quality control, and therefore, necessitate comprehensive RNA surveillance (33–36). Currently, the precise contributions of RNA surveillance to cellular reprogramming remain to be elucidated. In addition, how to harness RNA surveillance for a better control of cell fates? Definitely, it will have broad applications if we can control the expression levels of RNA exosome components at a whole with small molecules rather than genetic tool.

Here, we carry out a chemical screening and find that RXRα-specific agonist CD3254 can significantly promote chemical reprogramming of fibroblasts. Further mechanistic studies provide interesting findings that CD3254–RXRα axis can transcriptionally activate RNA exosome with all the 11 components in total, including *Exosc1–10* and *Dis3*. Unexpectedly, RNA exosome mainly regulates the degradation of transposable element (TE)-associated repeat RNAs, particularly *MMVL30-int*, which functions as a new barrier for cellular reprogramming. In turn, the degradation of *MMVL30* mediates the reduction of inflammation, contributing to the promotion of chemical reprogramming. Overall, these studies provide us a better understanding of cell-fate transitions.

Results

Identification of CD3254 That Can Significantly Promote Chemical Reprogramming. Chemical reprogramming provides a unique assay to investigate the interplay between environmental cues and cell-fate decisions. However, chemical reprogramming is a slow and inefficient process and takes about 40 days in total with multiple stages (Stages 1 to 3). Therefore, we decided to identify small molecules to improve the reprogramming technology, which is still in its infancy. A mouse chemical reprogramming protocol recently refined in our lab was applied as a starting point for screening (10). Briefly, we used OG2 MEFs as starting materials, treated cells with Stage 1 medium from day 0 to day 12, and screened small molecules during Stage 1, using Sall4-positive colony number as readout (Fig. 1*A*). Interestingly, CD3254 was the top candidate, and the effect could be further confirmed (Fig. 1 *B*–*D*). Next, we extended the reprogramming process to Stage 2 and observed the increase of p*Oct4*-GFP-positive colony number (Fig. 1 *E* and *F*). The optimal concentration of CD3254 was 0.5 μM, and additionally, CD3254 mainly functioned at Stage 1 (Fig. 1 *G* and *H*). Using real-time quantitative PCR (RT-qPCR), we observed that CD3254 induced the expression of early pluripotent genes, including *Sall4*, *Cdh1*, *Epcam*, and *Lin28a* (Fig. 1*I*). Other RXR agonists bexarotene and SR11237 could also significantly enhance reprogramming (*SI Appendix*, Fig. S1 *A* and *B*), while RXR antagonist HX531 blocked the effect of CD3254 (*SI Appendix*, Fig. S1 *C* and *D*). In addition, CD3254 enhanced the efficiency of chemical reprogramming, rather than the kinetics (*SI Appendix*, Fig. S1*E*). We further applied CD3254 to transcription factor (TF)-mediated reprogramming and observed a limited effect (*SI Appendix*, Fig. S1*F*). Overall, through chemical screening, we have identified a unique small molecule CD3254, a specific and potent RXRα agonist, that could significantly enhance the efficiency of chemical reprogramming, overcoming one challenging issue of chemical reprogramming. Based on these strong and replicable effects, we decided to focus our following studies on CD3254 for a better understanding of chemical reprogramming, which remains largely unexplored.

After further culturing the day-24 reprogramming intermediates for another 12 to 16 d, we established several p*Oct4*-GFP-positive ciPSC lines and characterized them in detail (Fig. 2*A*). These p*Oct4*-GFP-positive cells had the typical mouse ESC morphology (Fig. 2*B*). Immunostaining demonstrated that these ciPSCs expressed typical pluripotent markers, including Oct4, Sox2, and Nanog (Fig. 2*C*). RT-qPCR showed the robust expression of pluripotency genes, such as *Oct4*, *Sox2*, and *Nanog* (Fig. 2*D*). RNA-Seq suggested that these ciPSCs are similar to mESCs at transcriptome level (Fig. 2*E*). Bisulfite sequencing analysis revealed that the *Oct4* and *Nanog* promoters of these ciPSCs were largely demethylated, providing further evidence for the successful epigenetic rewiring (Fig. 2*F*). Karyotyping results showed that these ciPSCs maintained a normal karyotype (Fig. 2*G*). By embryoid body differentiation, we could observe all the three germ layer cells, such as Tuj1-positive ectoderm, α-SMA-positive mesoderm, and Foxa2-positive endoderm (Fig. 2*H*). Teratoma assay showed that these ciPSCs could generate typical teratomas containing derivatives of all the three germ layers, including ectoderm, mesoderm, and endoderm (Fig. 2*I*). CD3254–ciPSCs also could generate chimeric mice (Fig. 2*J*), further addressing the pluripotency in vivo. In aggregate, the above comprehensive characterizations demonstrated that these ciPSCs are molecularly and functionally similar to mESCs, proving the successful pluripotent reprogramming by a chemical approach.

Transcriptional Analysis of the Effects of CD3254 on Chemical Reprogramming. To identify the molecular mechanisms of CD3254 in chemical reprogramming, the reprogramming intermediates treated with and without CD3254 were harvested to perform RNA-Seq. The datasets were replicable (*SI Appendix*, Fig. S2*A*). Next, we conducted differential gene expression analysis between the two treatment conditions. In total, 1,330 genes were up-regulated and 1,330 genes were down-regulated after CD3254 treatment (fold change >1.5 or <0.67, adjusted *P*-value < 0.05) (Figs. 3*A* and *SI Appendix*, Fig. S2*B*). Next, we did Kyoto Encyclopedia of Genes and Genomes (KEGG) pathway enrichment analysis. The KEGG terms among up-regulated genes included DNA replication, homologous recombination, spliceosome, and RNA degradation (Fig. 3*B*). The down-regulated KEGG terms included steroid biosynthesis, MAPK signaling pathway, focal adhesion, and TGF-beta signaling (Fig. 3*C*). In particular, early pluripotency genes (e.g., *Sall4*, *Lin28a*, *Esrrb*, *Klf4*, *cMyc*) and epithelial genes (e.g., *Cdh1*, *Cldn4*, *Tjp3*) were up-regulated, while mesenchymal genes (e.g., *Zeb1*, *Twist1*, *Snail1*) were down-regulated (Fig. 3 *D*–*F*). We also observed the downregulation of key genes involved in TGF-beta signaling pathway (e.g., *Tgfb1*, *Grem1*, *Smad3*) (Fig. 3*G*). In addition, gene ontology (GO) analysis showed up-regulated terms, including stem cell population maintenance, chromatin organization, RNA metabolic process, and DNA replication. Down-regulated GO terms included exocellular matrix, epithelial-to-mesenchymal transition, TGF-beta, and MAPK signaling pathway (Fig. 3*H*). Gene set enrichment analysis (GSEA) results further suggested the upregulation of ribosome, spliceosome, DNA repair, pyrimidine metabolism, and downregulation of lysosome, cytokine–cytokine receptor interaction, and Hedgehog signaling pathway (*SI Appendix*, Fig. S2*C*). Overall, CD3254 treatment promotes the rewiring of gene regulatory network, accelerating MET and pluripotency induction.

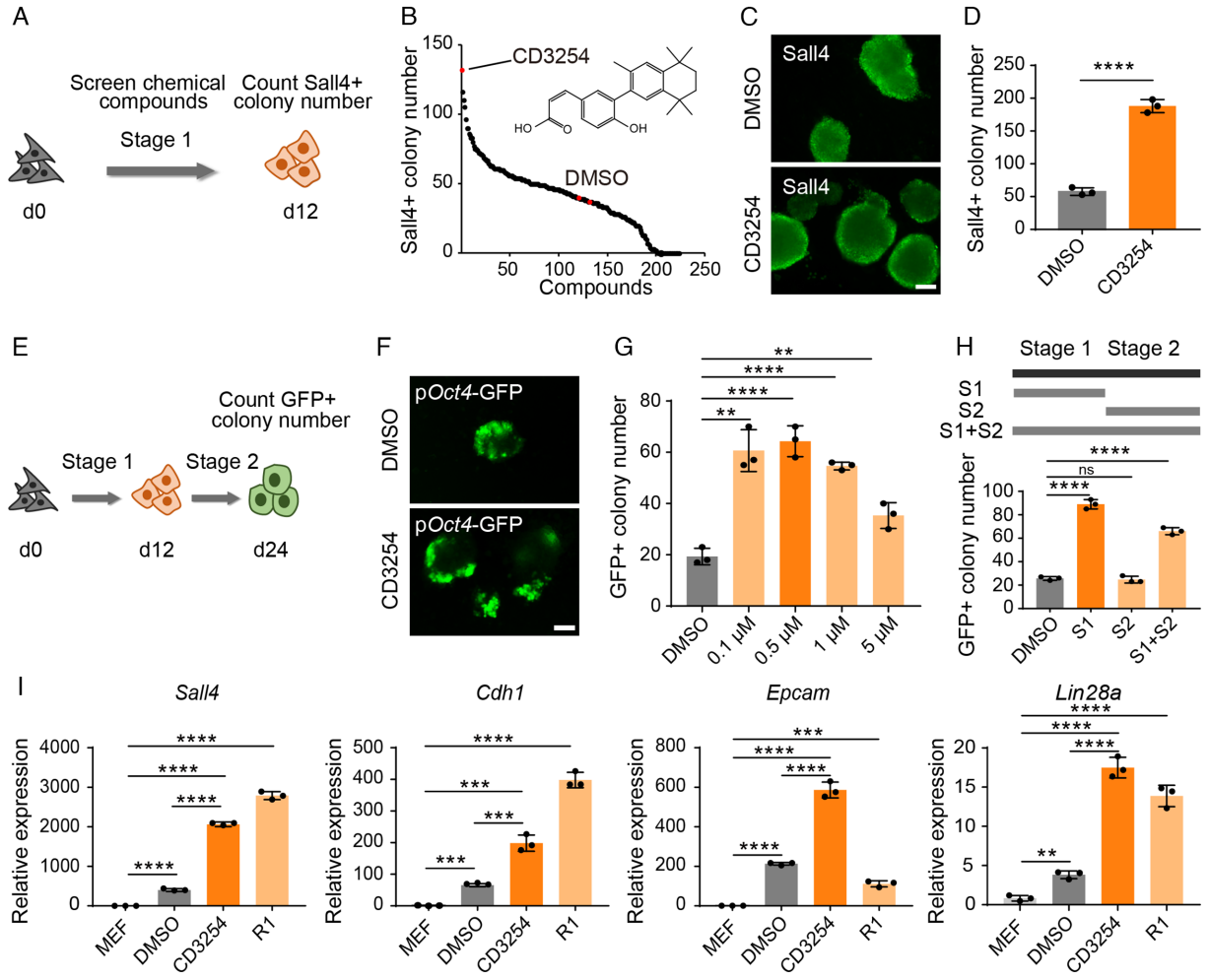

Fig. 1. RXRα agonist CD3254 can significantly promote mouse chemical reprogramming. (*A*) A schematic of compound screening during mouse chemical reprogramming. (*B*) The chemical screening result evaluated by Sall4$^+$ colony number on d12. (*C*) Fluorescence image of Sall4$^+$ colonies after DMSO and CD3254 treatments. (Scale bar, 100 μm.) (*D*) Sall4$^+$ colony number treated with CD3254. (*E*) Diagram showing the procedure to obtain p*Oct4*-GFP$^+$ colonies. (*F*) Fluorescence image of p*Oct4*-GFP$^+$ colonies after DMSO and CD3254 treatments. (Scale bar, 100 μm.) (*G* and *H*) Concentration (*G*) and stage (*H*) tests of CD3254. (*I*) RT-qPCR analysis of *Sall4*, *Cdh1*, *Epcam*, and *Lin28a* gene expression in MEFs, intermediate cells on d12 treated with DMSO and CD3254, and R1 mESCs. Data are presented as mean ± SD of three independent experiments. $^{**}P < 0.01$, $^{***}P < 0.001$, $^{****}P < 0.0001$.

RXRα Overexpression Can Significantly Promote Chemical Reprogramming. To further dissect whether CD3254 promotes mouse chemical reprogramming through its cognate target RXRα, we tested the functions of *Rxra* knockdown and overexpression (Fig. 4 *A* and *B*). *Rxra* knockdown by shRNAs inhibited Sall4-positive colony number and the expression of early pluripotency marker genes, such as *Sall4*, *Cdh1*, *Epcam*, and *Lin28a* (Fig. 4 *C* and *D*). Unexpectedly, the effect of *Rxra* overexpression was even more significant, and could increase the number of Sall4-postive colonies by about 10-fold, further suggesting that CD3254–RXRα axis plays critical roles in chemical reprogramming (Fig. 4 *E*–*G*).

Again, using RNA-Seq, we evaluated the gene expression changes by *Rxra* overexpression. In total, 1,953 genes were up-regulated and 2,147 genes were down-regulated after *Rxra* overexpression (fold change > 1.5 or < 0.67, adjusted *P*-value < 0.05) (Fig. 5*A*, and *SI Appendix*, Fig. S3 *A* and *B*). The up-regulated categories included stem cell population maintenance, chromatin remodeling, DNA replication, RNA degradation, and mRNA surveillance pathway (Fig. 5*B* and *SI Appendix*, Fig. S3*D*). On the contrary, the down-regulated genes belonged to the categories of lysosome, focal adhesion, MAPK signaling pathway, TGF-beta signaling pathway, autophagy, and response to hypoxia (*SI Appendix*, Fig. S3 *C* and *D*). Similar to CD3254 treatment, we found that early pluripotency genes and epithelial genes were up-regulated, while mesenchymal genes and key genes involved in TGF-beta signaling pathway were down-regulated (*SI Appendix*, Fig. S3*F*). GSEA further suggested the upregulation of homologous recombination, and downregulation of cytokine–cytokine receptor interaction, lysosome, and chemokine signaling pathway (*SI Appendix*, Fig. S3*E*). Overall, *Rxra* overexpression also enhances (even more efficiently than CD3254) the rewiring of gene regulatory network from somatic to pluripotent state.

CD3254–RXRα Axis Transcriptionally Up-regulates RNA Exosome. Integrating the RNA-Seq datasets of CD3254 treatment and *Rxra* overexpression, we found that RNA exosome component genes were notably induced. RNA exosome is a complex of 11 subunits in total and involved in RNA degradation (28, 29) (Fig. 5 *B* and *C*). The roles of RNA exosome in cellular reprogramming have not been described and remain largely unknown. As shown in Fig. 5*D*, both CD3254 treatment and *Rxra* overexpression increased the expression of all the 11 subunits of RNA exosome, including *Exosc1–10* and *Dis3*. We used RT-qPCR to further confirm the upregulation of *Exosc3*, *Exosc7*, *Exosc8*, and *Dis3* after CD3254 treatment and *Rxra* overexpression (Fig. 5 *E* and *F*). In addition, both CD3254 treatment and *Rxra* overexpression could

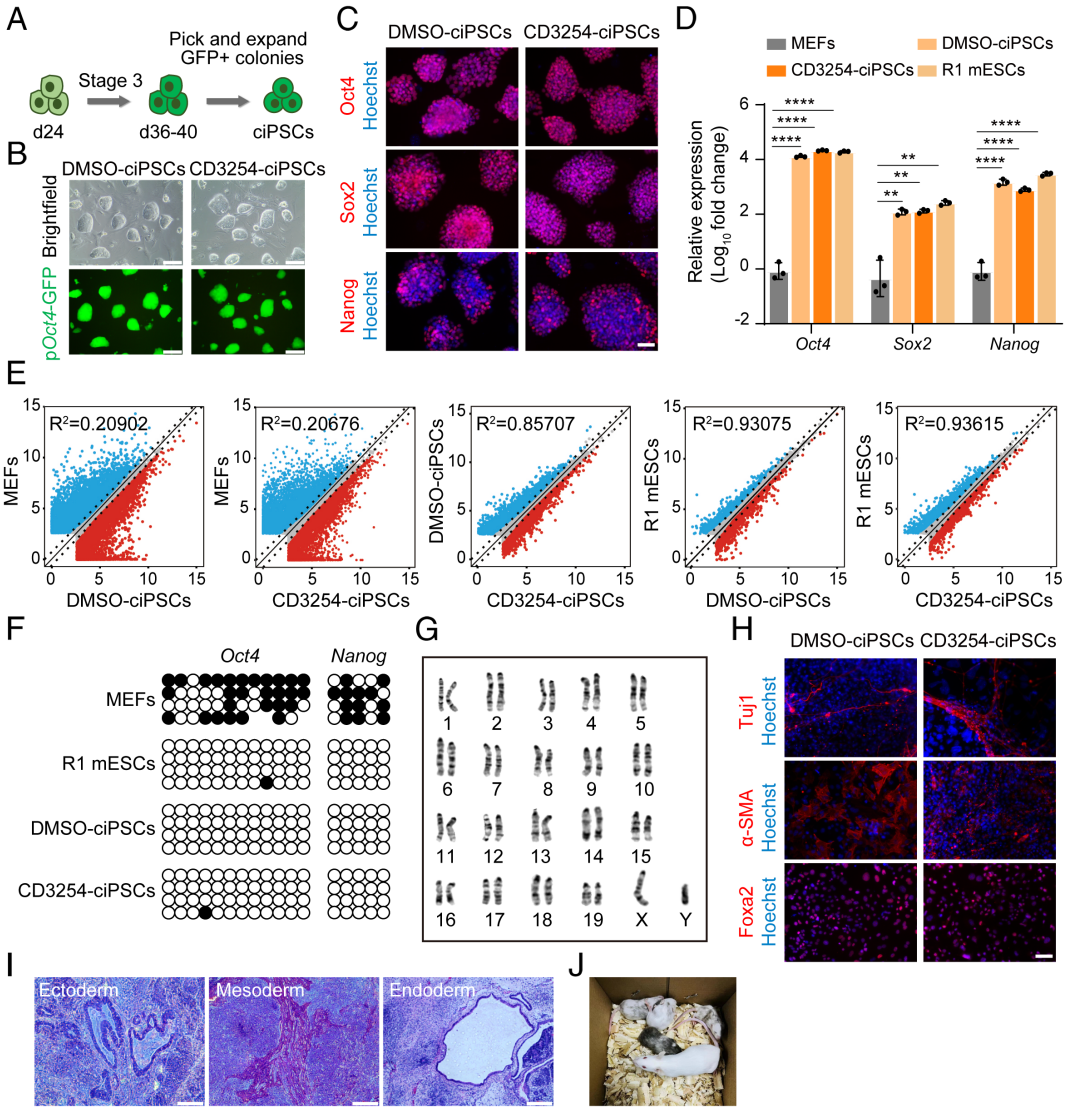

Fig. 2. Characterization of ciPSCs. (*A*) Schematic diagram of establishing ciPSC lines. (*B*) Brightfield and p*Oct4*-GFP pictures of ciPSCs generated with DMSO and CD3254 treatments at Stage 1. (*C*) Immunofluorescence analysis of pluripotency markers. (Scale bar, 50 μm.) (*D*) RT-qPCR analysis of *Oct4*, *Sox2*, and *Nanog* gene expression. (*E*) Scatter plots comparing the transcriptomes of MEFs, ciPSCs, and R1 mESCs. (*F*) Bisulfite sequencing analysis of the DNA CpG methylation of the *Oct4* and *Nanog* promoter loci. (*G*) Karyotyping analysis of ciPSCs. (*H*) Immunofluorescence analysis of three germ layer differentiation markers. (Scale bar, 100 μm.) (*I*) Hematoxylin and eosin staining showing the ectoderm, mesoderm, and endoderm components from the teratoma of ciPSCs. (Scale bar, 100 μm.) (*J*) Chimeric mice generated by ciPSCs. Data are presented as mean ± SD of three independent experiments. $^{**}P < 0.01$, $^{****}P < 0.0001$.

up-regulate the protein levels of Exosc3 and Dis3 (*SI Appendix*, Fig. S3*G*).

We conducted transcription factor (TF) regulatory potential index analysis of RNA exosome component genes using Cistrome database, and RXRα was identified as a predictive upstream regulatory TF of RNA exosome component genes (*SI Appendix*, Fig. S4 *A* and *B*). To determine whether RNA exosome subunit genes are the direct downstream targets of RXRα, we performed CUT&Tag assay (23). Indeed, we observed that RXRα could directly bind to the genomic regions of all the 11 RNA exosome component genes (Fig. 5 *G* and *H* and *SI Appendix*, Fig. S4*C*). Next, the direct binding of RXRα on the genomic regions of RNA exosome component genes *Exosc3* and *Dis3* was further confirmed by CUT&Tag-qPCR assay (Fig. 5 *I* and *J*). In sum, we have identified RXRα as a direct upstream regulator of all component genes of RNA exosome.

RNA Exosome Is Required for Chemical Reprogramming. Next, we tested the function of RNA exosome in chemical reprogramming. We used shRNAs to knock down *Exosc3*, a core component of RNA exosome (Fig. 6 *A* and *B*). We found that *Exosc3* knockdown decreased the number of Sall4-positive colonies and the expression of early pluripotency maker genes *Sall4*, *Cdh1*, *Epcam*, and *Lin28a* (Fig. 6 *C* and *D*). Additionally, knockdown of *Dis3*, another key component of RNA exosome, demonstrated a similar phenotype (*SI Appendix*, Fig. S5 *A–D*). Using RNA-Seq, we evaluated the gene expression changes after *Exosc3* knockdown. In total, 314 genes were up-regulated and 1,093 genes were down-regulated after *Exosc3* knockdown (fold change > 1.5 or < 0.67, adjusted *P*-value < 0.05) (Fig. 6 *E* and *F*). The up-regulated genes belong to terms of ECM–receptor interaction, response to wounding, and cytokine–cytokine receptor interaction (Fig. 6 *G* and *I*). On the contrary, the down-regulated terms included DNA replication, chromatin organization, glycine, serine and threonine metabolism, and signaling pathways regulating pluripotency of stem cells (Fig. 6 *H* and *I*). Taken together, we have identified that RNA exosome is a positive regulator for chemical reprogramming.

RNA Exosome Mainly Targets Repeat RNAs for Degradation. The overall much higher number of down-regulated mRNAs (314 up versus 1,093 down) after *Exosc3* knockdown is counterintuitive,

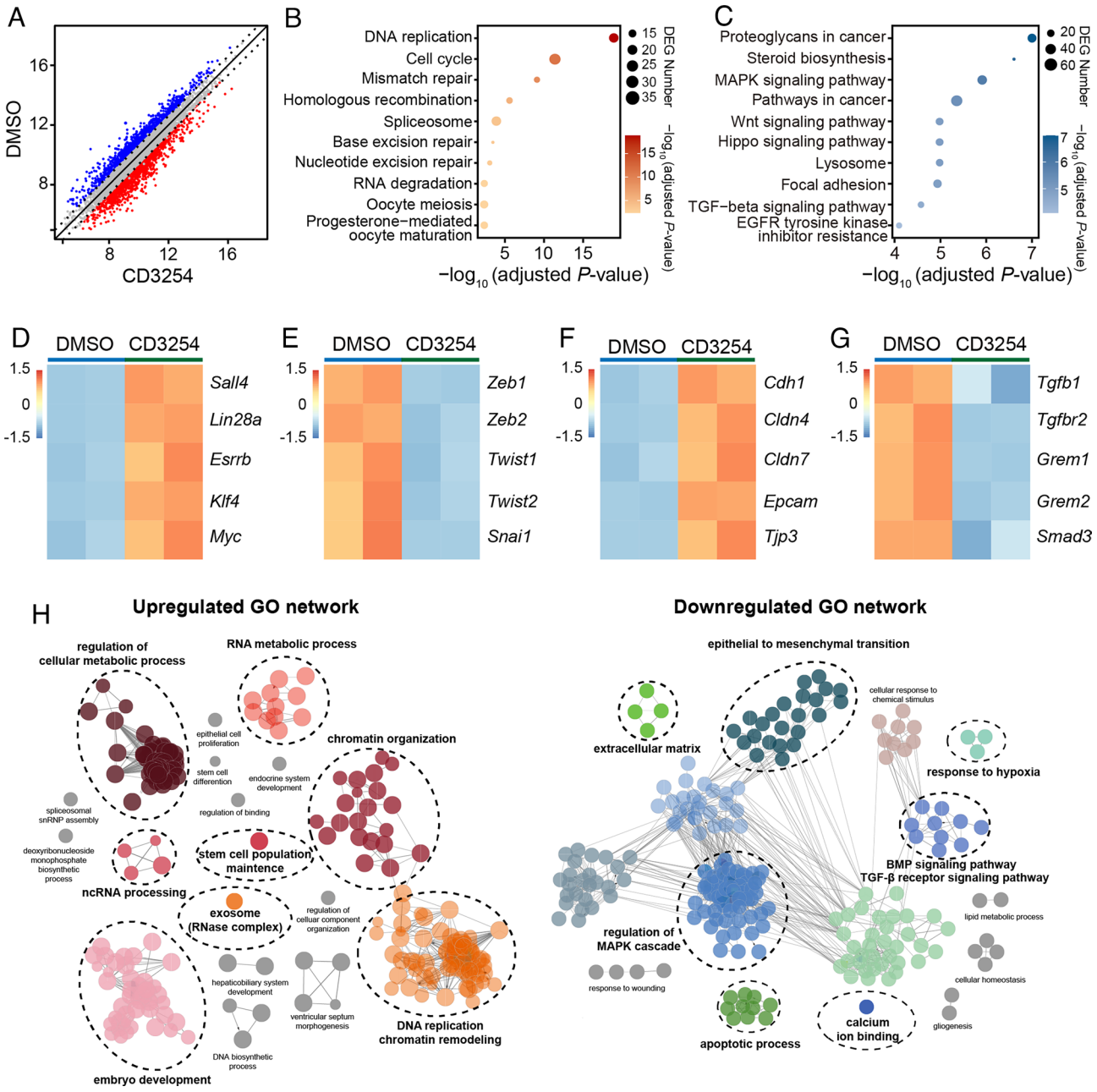

Fig. 3. Transcriptional analysis of the effects of CD3254 on chemical reprogramming. (*A*) Scatter plots comparing global gene expression patterns between CD3254 and DMSO cells. The red dots (n = 1,330) and blue dots (n = 1,330) represent up-regulated (FC > 1.5) and down-regulated (FC < 0.67) differentially expressed genes with statistical significance (adjusted *P*-value < 0.05), respectively. (*B* and *C*) Bubble plots of KEGG pathways enriched in up-regulated (*B*) and down-regulated (*C*) genes in CD3254 vs. DMSO cells. Cycle size represents the gene numbers in each pathway, orange or blue gradient represents the adjusted *P*-value of each pathway. *P*-values were calculated by one-tailed hypergeometric test. (*D*–*G*) Expression heatmaps of early pluripotent (*D*), mesenchymal (*E*), epithelial (*F*), and TGF-β signaling pathway (*G*)-related genes in CD3254 and DMSO cells. (*H*) Functional enrichment analysis of up-regulated (*Left*) and down-regulated (*Right*) genes in CD3254 vs. DMSO cells. Black cycles represent the main GO term clusters among differentially expressed genes.

as RNA exosome is an RNA degrader. Such observation is also distinct from previous observations in other biological systems (31, 35, 37). Besides mRNAs, noncoding RNAs (ncRNAs) including long noncoding RNAs (lncRNAs), enhancer RNAs (eRNAs), promoter-associated RNAs (paRNAs), and transposable element-associated RNAs (repeat RNAs) have also been shown as the substrates of RNA exosome (31, 35, 37). To investigate the effects of RNA exosome on ncRNAs, we quantified the expressional changes of lncRNAs, eRNAs, and paRNAs upon *Exosc3* knockdown. Overall, the expression levels of these ncRNAs showed downward trends in sh*Exosc3*, similar with mRNAs (*SI Appendix*, Fig. S6 *A*, *E*, and *F*). Moreover, we observed that the expression patterns of some lncRNAs are in correlation with that of the nearby genes, indicating the close expressional regulation of the lncRNAs on their nearby genes. For example, after *Exosc3* knockdown, the expression of *Gm14261*, which is upstream of *Sall4*, was decreased, and the expression of *Gm10638* located at downstream of *Siah1a* was increased (*SI Appendix*, Fig. S6 *B*–*D*).

Unexpectedly, the expression of repeat RNAs was significantly increased upon *Exosc3* knockdown, suggesting that RNA exosome mainly targets repeat RNAs for degradation during reprogramming (Fig. 7*A*). We discovered that majority of the differentially expressed repeat RNAs were up-regulated (n = 3,403), while only a few were down-regulated (n = 35) (Fig. 7*B*). The increased repeat RNAs included the majority of TE classes, such as long terminal repeat (LTR)-containing endogenous retroviruses (ERVs) and

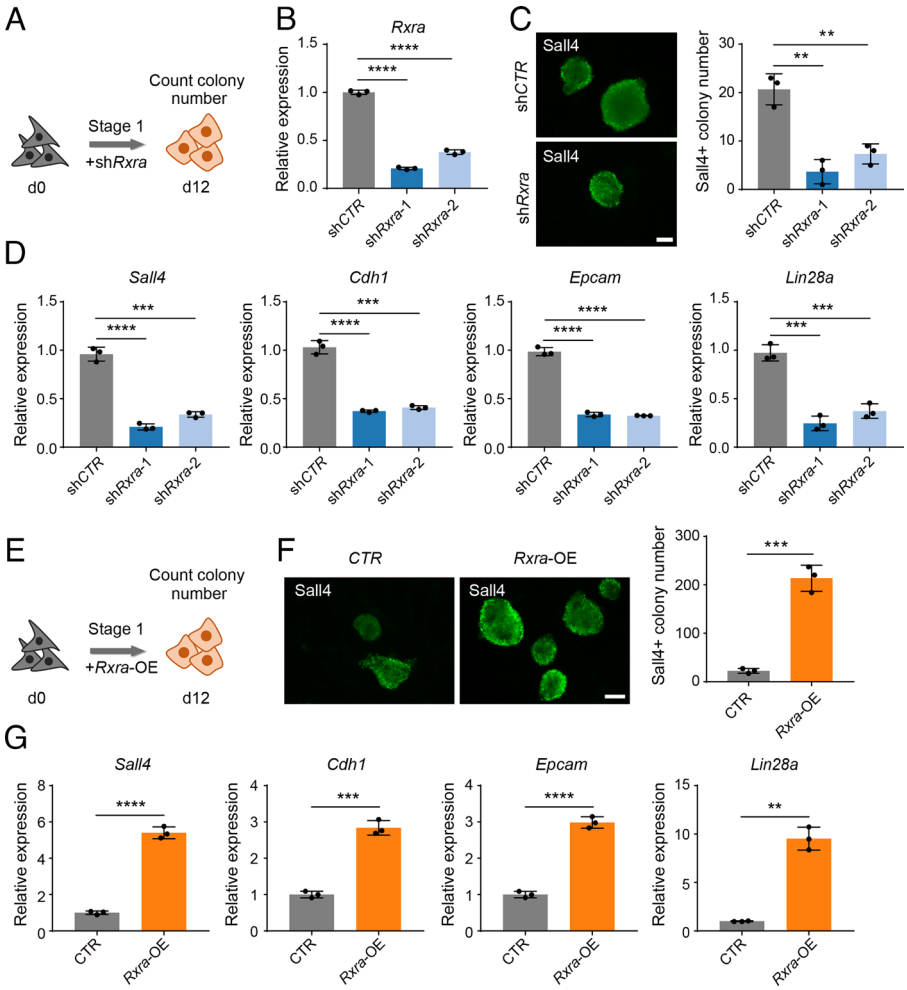

Fig. 4. RXRα enhances mouse chemical reprogramming. (*A*) Diagram showing the procedure of *Rxra* knockdown. (*B*) RT-qPCR analysis of *Rxra* expression in MEFs infected with sh*CTR* and sh*Rxra* viruses. (*C*) Immunofluorescence of Sall4 in reprogramming intermediates infected with sh*CTR* and sh*Rxra* viruses. (Scale bar, 100 μm.) (*D*) RT-qPCR analysis of pluripotent gene expression in cells treated with sh*CTR* and sh*Rxra*. (*E*) Diagram showing the procedure of reprogramming infected with *Rxra*-OE viruses. (*F*) Immunofluorescence of Sall4 in control cells and *Rxra* overexpressing cells on d12. (Scale bar, 100 μm.) (*G*) RT-qPCR analysis of pluripotent gene expression in cells treated with *CTR* and *Rxra*-OE. Data are presented as mean ± SD of three independent experiments. $^{**}P < 0.01$, $^{***}P < 0.001$, $^{****}P < 0.0001$.

non-LTR elements, including long interspersed nuclear elements (LINEs) and short interspersed nuclear elements (SINEs) (Fig. 7*C*). Interestingly, through precisely investigating the expressional changes of repeat RNAs, we found that eight out of the top 10 up-regulated repeat RNAs (ranked by $\log_2$ fold change and *P*-values) are *MMVL30-int*, which belongs to *VL30 ERV1* family (38) (Fig. 7 *B* and *C*). In addition, the proportion of the up-regulated *MMVL30-int* duplicates was significantly higher than that of the all expressed TEs, implying that *MMVL30-int* was the major target of RNA exosome (Fig. 7*D*). To further validate this hypothesis, we investigated the expressional changes of repeat RNAs after CD3254 treatment and *Rxra* overexpression. Again, *MMVL30-int* was significantly enriched in the high-ranking down-regulated TEs (*SI Appendix*, Fig. S6 *G* and *H*). Integrated analysis of these RNA-Seq datasets showed that 13 *MMVL30-int* duplicates were regulated by *Exosc3* knockdown, CD3254 treatment, and *Rxra* overexpression (Fig. 7*E*). The expression patterns of these duplicates showed distinct manners in CD3254 treatment, *Rxra* overexpression, and *Exosc3* knockdown, implying that RNA exosome is indeed responsible for degradation of *MMVL30-int* transcripts (Fig. 7 *F* and *G*). RT-qPCR confirmed the downregulation of *MMVL30* expression by CD3254 treatment and *Rxra* overexpression and the upregulation of *MMVL30* expression by *Exosc3* knockdown (Fig. 7*H*). Moreover, we performed Exosc3 RNA immunoprecipitation with RT-qPCR (RIP-qPCR) and validated that Exosc3 could directly bind *MMVL30* (Fig. 7*I*). Next, we analyzed the RNA-Seq data of reprogramming intermediates treated with transcription inhibitor actinomycin D (Act D) and collected at 0 h, 4 h, and 8 h. We found that the stability of *MMVL30-int* was significantly decreased in CD3254 treatment cells (Fig. 7*J*). Functionally, we found that *MMVL30* knockdown could increase Sall4-positive colonies (Fig. 7*K* and *SI Appendix*, Fig. S7 *A–C*) and promote the induction of early pluripotent genes, including *Sall4*, *Cdh1*, *Epcam*, and *Lin28a* (*SI Appendix*, Fig. S7*D*). Therefore, *MMVL30* functions as a new barrier for chemical reprogramming.

Collectively, by further data exploration, we identified that CD3254–RXRα–RNA exosome axis promotes the degradation of transposable element (mainly *MMVL30*) during cell-fate transitions.

RNA Exosome-Mediated Transposable Element Degradation and Inflammation Reduction Promote Chemical Reprogramming. Recent studies have suggested that accumulation of *MMVL30* transcripts can stimulate cytoplasmic nucleotide sensing pathways, and subsequently, interferon response, which function in tumorigenesis, development, and tissue repair (39–41). However, the roles of TEs in cellular reprogramming remain elusive.

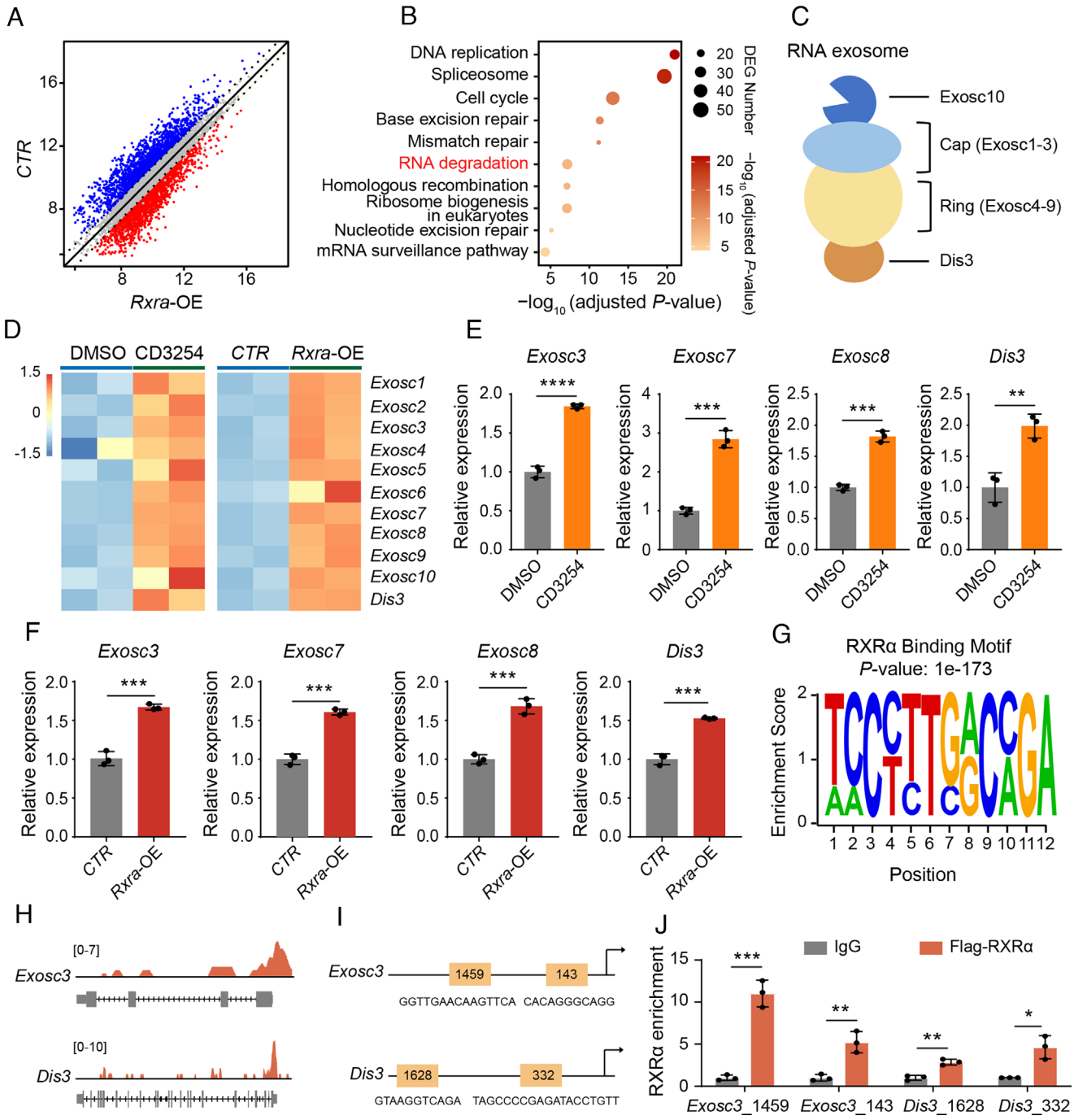

Fig. 5. CD3254–RXRα axis transcriptionally activates RNA exosome. (*A*) Scatter plots comparing global gene expression patterns between *Rxra*-OE and control cells. The red dots (n = 1,953) and blue dots (n = 2,417) represent up-regulated (FC > 1.5) and down-regulated (FC < 0.67) differentially expressed genes with statistical significance (adjusted *P*-value < 0.05), respectively. (*B*) Bubble plots of KEGG pathways enriched in up-regulated genes in *Rxra*-OE vs. control cells. Cycle size represents the gene numbers in each pathway, orange gradient represents the adjusted *P*-value of each pathway. RNA degradation pathway is highlighted in red font, *P*-values were calculated by one-tailed hypergeometric test. (*C*) A model of the exosome complex. This nine-subunit core exosome is composed of a three-subunit cap (Exosc1-3) at the top and a six-subunit ring (Exosc4-9) in the middle. Two active ribonuclease subunits, Dis3 and Exosc10, contact the bottom and top of this structure, respectively. (*D*) Expression heatmap of exosome-related genes. (*E* and *F*) RT-qPCR analysis of *Exosc3*, *Exosc7*, *Exosc8,* and *Dis3* expression in CD3254-treated (*E*) and *Rxra*-OE cells (*F*) on d12. (*G*) Representation of the RXRα-binding motif; *P*-value was calculated by one-tailed hypergeometric test. (*H*) Browser tracks displaying the RXRα peaks at *Exosc3* and *Dis3* loci. (*I*) The predicted RXRα-binding sites at the promoters of *Exosc3* and *Dis3*. (*J*) RT-qPCR analysis of the binding capacity of RXRα at *Exosc3* and *Dis3* gene loci. Data are presented as mean ± SD of three independent experiments. **P* < 0.05, ***P* < 0.01, ****P* < 0.001, *****P* < 0.0001.

Therefore, we decided to further explore the consequences after the dysregulation of *MMVL30* during chemical reprogramming.

Overall, we found that a number of ERVs were induced in the forms of both sense and antisense transcripts upon *Exosc3* knockdown (Fig. 8*A*). These up-regulated ERVs, including *MMVL30-int*, were expressed in both forward and reverse orientations and could form double-stranded RNAs (dsRNAs) (Fig. 8*B*). Indeed, fluorescence-activated cell sorting (FACS) analysis identified that CD3254 treatment could decrease the total dsRNA level (Fig. 8*C*). We also observed the reduction of dsRNAs formed by *MMVL30* (Fig. 8*D*). The accumulation of dsRNAs can trigger inflammation and immune response (39, 40, 42). Indeed, we observed that several inflammation-related genes, including *Ifngr1*, *Tnfrsf1a*, and *Tnfrsf10b,* were down-regulated in the CD3254-treated, *Rxra*

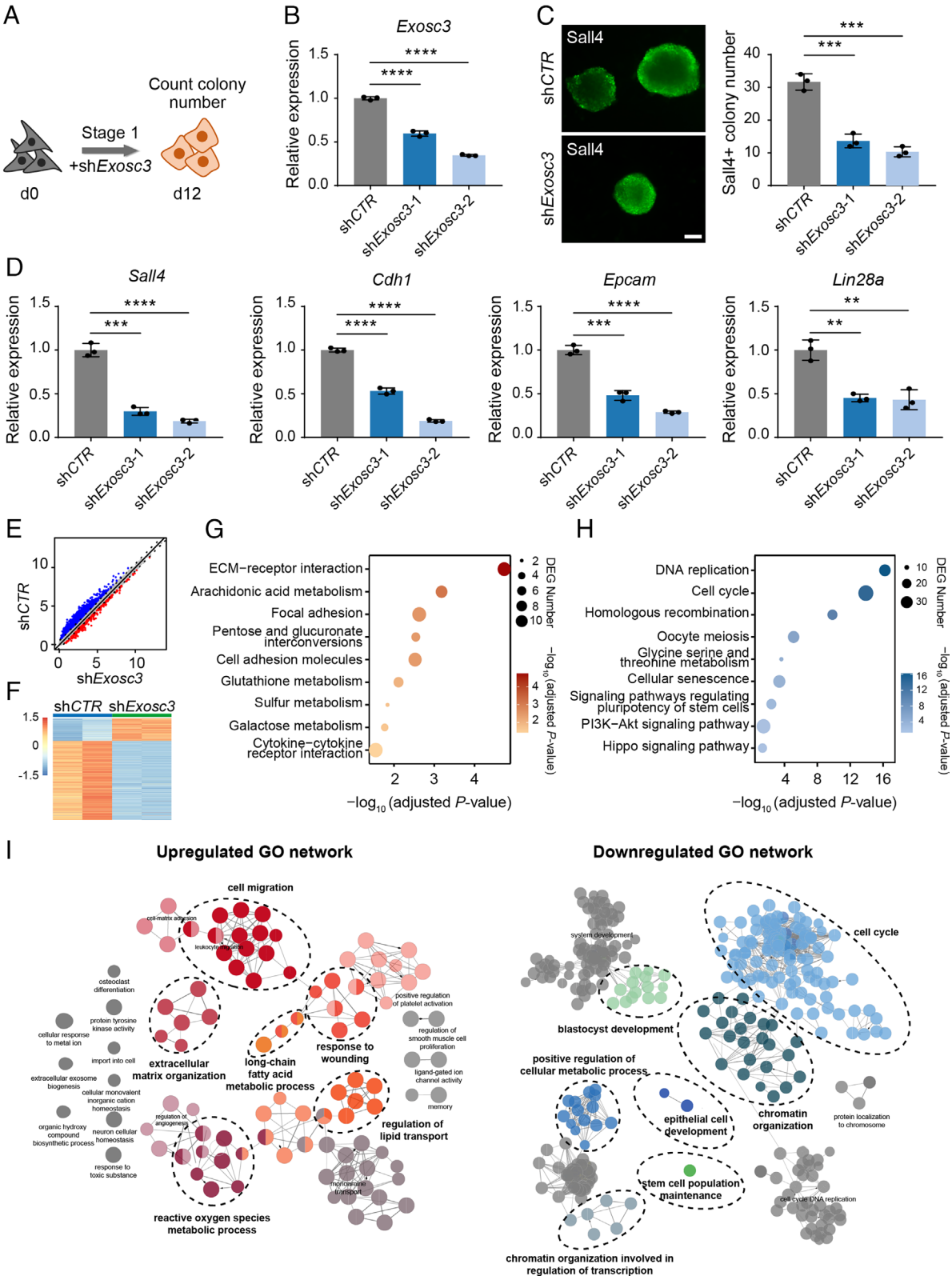

Fig. 6. RNA exosome is essential during reprogramming to pluripotency. (*A*) Diagram showing the procedure of *Exosc3* knockdown. (*B*) RT-qPCR analysis of *Exosc3* expression in MEFs infected with sh*CTR* and sh*Exosc3* viruses. (*C*) Immunofluorescence of Sall4 in reprogramming intermediates infected with sh*CTR* and sh*Exosc3* viruses. (Scale bar, 100 μm.) (*D*) RT-qPCR analysis of pluripotent gene expression in cells treated with sh*CTR* and sh*Exosc3*. (*E*) Scatter plots comparing global gene expression patterns between sh*Exosc3* and sh*CTR* cells. The red dots (n = 314) and blue dots (n = 1,093) represent up-regulated (FC > 1.5) and down-regulated (FC < 0.67) differentially expressed genes with statistical significance (adjusted *P*-value < 0.05), respectively. (*F*) Expression heatmap of differentially expressed mRNAs in sh*Exosc3* and sh*CTR* cells. (*G* and *H*) Bubble plots of KEGG pathways enriched in up-regulated (*G*) and down-regulated (*H*) genes in sh*Exosc3* vs. sh*CTR* cells. Cycle size represents the gene numbers in each pathway, orange or blue gradient represents the adjusted *P*-value of each pathway, and *P*-values were calculated by one-tailed hypergeometric test. (*I*) Functional enrichment analysis of up-regulated (*Left*) and down-regulated (*Right*) genes in sh*Exosc3* vs. sh*CTR* cells. Black cycles represent the main GO term clusters among differentially expressed genes. Data are presented as mean ± SD of three independent experiments. ***P* < 0.01, ****P* < 0.001, *****P* < 0.0001.

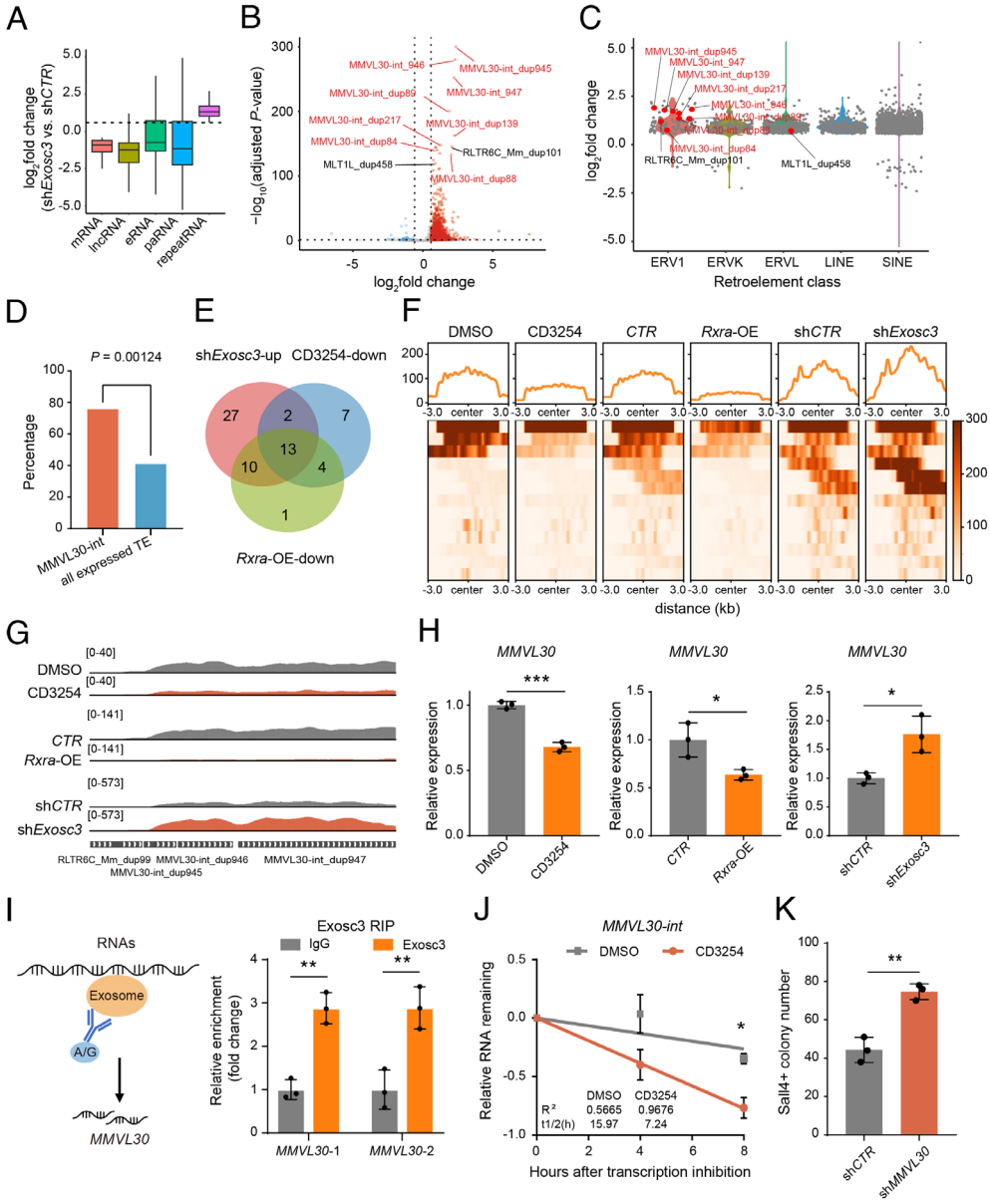

Fig. 7. RNA exosome targets transposable element-associated RNAs for degradation. (*A*) Box plot showing the $\log_2$ fold changes for different types of differentially expressed RNAs. In box plot, lower and upper hinges represent first and third quartiles, respectively, the center line represents the median, and whiskers represent ±1.5× the interquartile range. (*B*) Volcano plot showing the differentially expressed retroelement duplicates in sh*Exosc3* vs. sh*CTR* cells. Red dots: 3,403 up-regulated repeat RNAs (FC > 1.5, adjusted *P*-value < 0.05), blue dots: 35 down-regulated repeat RNAs (FC < 0.67, adjusted *P*-value < 0.05). Top significantly up-regulated TE duplicates are labeled (FC > 2, adjusted *P*-value < $1e^{-100}$). *MMVL30-int* duplicates are highlighted in red font. (*C*) The differentially expressed retroelement classes comparing sh*Exosc3* with sh*CTR* cells (FC > 1.5 or < 0.67, adjusted *P*-value < 0.05). *MMVL30-int* duplicates are highlighted in red font. (*D*) The Fisher's exact test showing the expression of *MMVL30-int* duplicates is significantly up-regulated in sh*Exosc3* vs. sh*CTR* cells. (*E*) Venn diagram showing the overlapped differentially expressed *MMVL30-int* duplicates in sh*Exosc3* vs. sh*CTR* (up-regulated), CD3254 vs. DMSO (down-regulated) and *Rxra*-OE vs. *CTR* (down-regulated) cells. (*F*) Density plots and heatmaps of 13 overlapped *MMVL30-int* duplicates' RNA abundance. RNA abundance on *MMVL30-int* duplicates was sorted by intensity. (*G*) Browser tracks showing some representative *MMVL30-int* duplicates (*MMVL30-int_dup945* to *dup947*) have decreased expression in CD3254-treated and *Rxra*-OE cells and increased expression in sh*Exosc3* cells. (*H*) RT-qPCR analysis of *MMVL30-int* expression in CD3254-treated, *Rxra*-OE, and sh*Exosc3* cells. (*I*) RIP-qPCR analysis of the *MMVL30* bound with Exosc3. (*J*) The decay curves for *MMVL30-int*. (*K*) Sall4$^+$ colonies in reprogramming intermediates treated with sh*CTR* and sh*MMVL30*. Data are presented as mean ± SD of three independent experiments. **P* < 0.05, ***P* < 0.01, ****P* < 0.001.

overexpression, and *MMVL30* knockdown samples, but, on the contrary, up-regulated in the *Exosc3* knockdown samples (Fig. 8*E*). To further test the roles of IFN-γ and TNF-α pathways, we added IFN-γ and TNF-α during reprogramming and found that they indeed decreased the number of Sall4-positive colonies (Fig. 8*F*). IFN-γ and TNF-α treatment down-regulated early pluripotent gene *Sall4* and epithelial gene *Cdh1*, while up-regulated mesenchymal gene *Zeb2* (Fig. 8*G*). On the contrary, JAK inhibitor upadacitinib and IKK inhibitor BMS-345541 could promote reprogramming (Fig. 8 *H* and *I*). The relationships between inflammation and cell fates are context dependent. Initial studies suggested that activation of TLR3- or IL6-mediated innate immunity is required for efficient pluripotent reprogramming (43–45). Later, several reports have suggested that IFN-γ- or TRAIL-mediated inflammation is a barrier for TF-induced pluripotency (46, 47). Here, our study indicated IFN-γ and TNF-α pathways as a roadblock of chemical reprogramming.

In summary, through unbiased chemical screening, we found that RXRα-specific agonist CD3254 can significantly promote chemical reprogramming. Further mechanistic studies provided interesting findings that CD3254–RXRα axis can transcriptionally activate RNA exosome with all the 11 components (*Exosc1–10* and *Dis3*) in

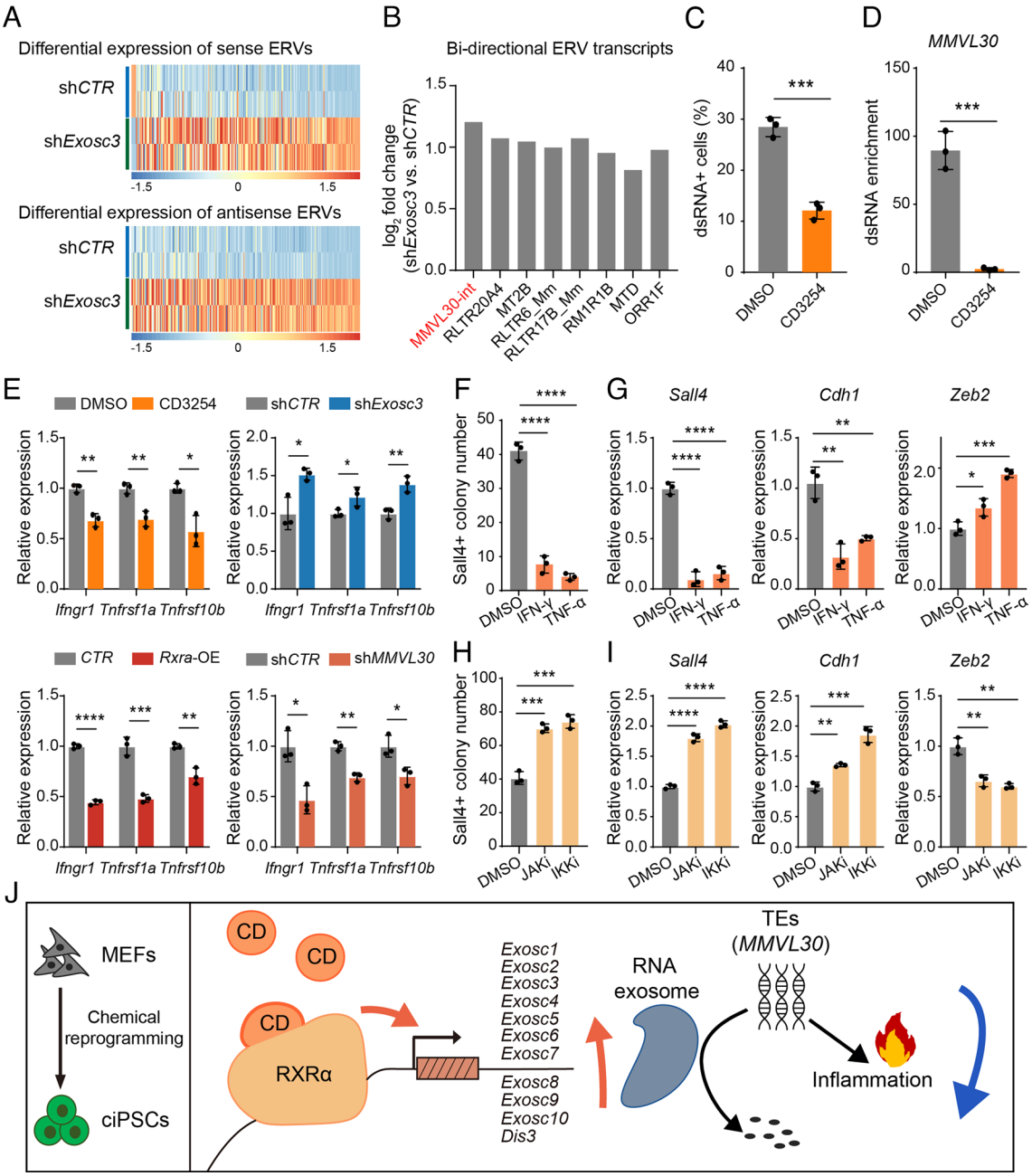

Fig. 8. *MMVL30* degradation by RNA exosome and subsequent inflammation reduction promote chemical reprogramming. (*A*) Expression heatmaps for differential expression (FC > 1.5 or < 0.67, adjusted *P*-value < 0.05) of sense or antisense transcripts of ERVs between sh*CTR* and sh*Exosc3* cells. (*B*) Bar plot showing the $\log_2$ fold changes of a number of representative bi-directional ERV transcripts in sh*Exosc3* vs. sh*CTR* cells. (*C*) CD3254 treatment down-regulated dsRNAs in reprogramming intermediates. (*D*) CD3254 reduced *MMVL30* dsRNAs. (*E*) RT-qPCR evaluation of *Ifngr1*, *Tnfrsf1a,* and *Tnfrsf10b* expression in CD3254-treated, *Rxra*-OE, and sh*Exosc3* cells. (*F*) Sall4$^+$ colonies with IFN-γ (20 ng mL^{-1}) and TNF-α (20 ng mL^{-1}) treatments. (*G*) RT-qPCR analysis of *Sall4*, *Cdh1*, and *Zeb2* expression with IFN-γ and TNF-α treatments. (*H*) Sall4$^+$ colonies with specific JAK inhibitor upadacitinib (5 μM) and IKK inhibitor BMS-345541 (1 μM) treatments. (*I*) RT-qPCR analysis of *Sall4, Cdh1*, and *Zeb2* expression with JAKi and IKKi treatments. (*J*) A summary diagram of this study. Data are presented as mean ± SD of three independent experiments. **P* < 0.05, ***P* < 0.01, ****P* < 0.001, *****P* < 0.0001.

total. After dissecting the exotome, we observed that RNA exosome mainly regulates the degradation of TEs (mainly *MMVL30-int* duplicates) and reduction of inflammation (e.g., IFN-γ and TNF-α pathways). Notably, these studies provided us insights into cell-fate transitions and better strategies to control cell fates (Fig. 8*J*).

Discussion

Compared to introducing exogenous transcription factors to abruptly forcing cells to change their identity, chemical approach is much less artificial by triggering innate cellular mechanisms. Here, through chemical screening, we identified CD3254 as a small molecule that can significantly promote mouse chemical reprogramming. Currently, chemical reprogramming is still in its infancy and has not been extensively studied. Particularly, unbiased chemical screening can provide us many unexpected findings and provide insights, as exemplified here and in our recent study of Syk inhibitor R406 in chemical reprogramming (10). Notably, our work is a good example for harnessing endogenous transcription factors directly by small molecules for efficient chemical reprogramming. These efforts will help us to develop efficient chemical reprogramming and to better understand the underlying molecular mechanisms.

Mechanistically, we demonstrated that CD3254–RXRα axis can transcriptionally activate RNA exosome with all the 11 components

in total. RNA exosome plays important roles in RNA surveillance and ensures precise control of RNA homeostasis in a spatiotemporally controlled manner and safeguards normal development (26, 28). Induction of RNA exosome at a whole by small molecule rather than genetic approach is very attractive. We foresee that it will be interesting to test whether activation of RNA exosome by CD3254 can be applied to other biological systems and further developed as therapeutics for various diseases, including injury and cancers. Previous studies mainly focused on mRNAs as the major targets of RNA exosome, and here, we found that RNA exosome mainly regulates the degradation of transposable elements (TEs), particularly *MMVL30*, which functions as a new barrier for cellular reprogramming.

In addition, *MMVL30*-mediated inflammation (IFN-γ and TNF-α pathways) is reduced, contributing to the promotion of chemical reprogramming. Previously, there are studies about the relationship between inflammation and cell fates. For example, initial studies suggested that activation of TLR3-mediated innate immunity is required for efficient pluripotent reprogramming (43). Later, injury-induced inflammation and senescence also modulate in vivo reprogramming (44, 45). Distinct to these studies, here we found that inflammation is a barrier for small molecule–induced mouse reprogramming. Therefore, the roles of inflammation in reprogramming are context dependent. Undoubtedly, these studies and further explorations will provide us better understanding of cell-fate transitions.

In summary, our studies not only have identified small molecules for improving the chemical reprogramming technique, but also identified unique molecular mechanisms, which opens areas for further exploration. In fact, the pluripotent reprogramming itself represents a valuable approach to study general mechanisms of cell-fate transitions. Deciphering the underlying molecular mechanisms of chemical reprogramming will generate fundamental insights into cell-fate decisions and in turn will provide innovative strategies to make the reprogramming process rapid and efficient, which can be applied for generating functional cells. Notably, these efforts will not only stimulate innovations for producing functional cells for regenerative medicine, but also provide unique approaches to pharmaceutically stimulate rejuvenation and regeneration in vivo.

Materials and Methods

Animals. OG2 mice and 129 mice were mated to generate offspring, which carried *Oct4* promoter-driven GFP reporter (OG2 x 129 mice). Mouse embryonic fibroblasts (MEFs) were obtained from E13.5 embryos of OG2 x 129 mice. The mice were housed in the pathogen-free facility of the Laboratory Animal Center of Zhejiang University and fed a normal chow diet. The animal-associated procedures used in this study were approved by the Experimental Animal Ethics Committee of Zhejiang University.

Cell Culture. MEFs and human embryonic kidney (HEK) 293T cells were maintained in DMEM containing 10% FBS and 1× penicillin/streptomycin (MEF medium). Mouse ESCs and ciPSCs were maintained on CF1 feeder cells in mESC medium containing DMEM, 10% KSR, 10% FBS, 1% NEAA, 0.055 mM 2-mercaptoethanol (β-ME), 1% P/S, 1,000 U mL^{-1} LIF, and the small molecules CHIR99021 (3 μM) and PD0325901 (0.2 μM). All cells were maintained in a humidified incubator at 37 °C and 5% CO_2.

ciPSC Generation. About 4 × 10^5 MEFs (at passage 3) were seeded onto one 24-well plate. After 24h, MEF medium was changed to Stage 1 medium: DMEM supplemented with 10% KSR, 10% FBS, 1% NEAA, 1% P/S, 0.055 mM β-ME, 20 ng mL^{-1} bFGF, and the small molecules VPA (0.5 mM), CHIR99021 (20 μM), 616452 (10 μM), parnate (5 μM), forskolin (50 μM), AM580 (0.5 μM), EPZ004777 (5 μM), and vitamin C (Vc) (250 μM). Stage 1 medium was changed every 4 d. On d12, the medium was switched to Stage 2 medium: DMEM supplemented with 10% KSR, 10% FBS, 1% NEAA, 1% P/S, 0.055 mM β-ME, 20 ng mL^{-1} bFGF, and the small molecules VPA (0.5 mM), CHIR99021 (10 μM), 616452, Parnate (5 μM), Forskolin (10 μM), AM580 (0.5 μM), DZNep (0.05 μM), 5-aza-dC (0.5 μM), SGC0946 (5 μM), and Vc (250 μM). Stage 2 medium was changed every 4 d for 12 d. On d24, Stage 3 medium was applied. Stage 3 medium contains 47% DMEM/F12, 47% neurobasal medium, 1× N2 supplement, 1× B27 supplement, 1% NEAA, 1% P/S, 0.055 mM β-ME, 1,000 U mL^{-1} LIF, and the small molecules CHIR99021 (3 μM) and PD0325901 (0.2 μM). Stage 3 medium was changed every 4 d for 12 to 16 d. Mouse ciPSC lines were generated from GFP^+ colonies with typical iPSC morphology. The information of reagents is listed in *SI Appendix*, Table S1.

Statistical Analysis. All experiments were performed with three replicates, and the data were presented as mean ± SD. Statistical significance was calculated using two-tailed Student's *t* test, which was presented as $*P < 0.05$, $**P < 0.01$, $***P < 0.001$, and $****P < 0.0001$.

Data, Materials, and Software Availability. All data have been deposited in the NCBI Gene Expression Omnibus database with accession number GSE208771 (48). All other study data are included in the article and/or *SI Appendix*.

ACKNOWLEDGMENTS. We thank members of Zhu lab for helpful discussions. This work was supported by the grants from National Natural Science Foundation of China (nos. 32270781 and 31970818), the National Key Research and Development Program of China (no. 2016YFC1305300), and the Outstanding Youth Fund of Zhejiang Province (no. R17C120002).

Author affiliations: [a]The Second Affiliated Hospital and Life Sciences Institute and School of Medicine, The Ministry of Education Key Laboratory of Biosystems Homeostasis and Protection and Zhejiang Provincial Key Laboratory for Cancer Molecular Cell Biology, Zhejiang University, Hangzhou 310058, China; [b]State Key Laboratory of Stem Cell and Reproductive Biology, Institute of Zoology, Chinese Academy of Sciences, University of Chinese Academy of Sciences, Beijing 100101, China; [c]Institute for Stem Cell and Regeneration, Chinese Academy of Sciences, University of Chinese Academy of Sciences, Beijing 100101, China; [d]Department of Endocrinology, Children's Hospital of Zhejiang University School of Medicine, Hangzhou 310052, China; and [e]Hangzhou Women's Hospital, Prenatal Diagnosis Center, Zhejiang University, Hangzhou 310008, China

1. T. Graf, Historical origins of transdifferentiation and reprogramming. *Cell Stem Cell* **9**, 504–516 (2011).
2. K. Takahashi, S. Yamanaka, Induction of pluripotent stem cells from mouse embryonic and adult fibroblast cultures by defined factors. *Cell* **126**, 663–676 (2006).
3. W. Li, K. Li, W. Wei, S. Ding, Chemical approaches to stem cell biology and therapeutics. *Cell Stem Cell* **13**, 270–283 (2013).
4. X. Ma, L. Kong, S. Zhu, Reprogramming cell fates by small molecules. *Protein Cell* **8**, 328–348 (2017).
5. P. Hou *et al.*, Pluripotent stem cells induced from mouse somatic cells by small-molecule compounds. *Science* **341**, 651–654 (2013).
6. Y. Zhao *et al.*, A XEN-like state bridges somatic cells to pluripotency during chemical reprogramming. *Cell* **163**, 1678–1691 (2015).
7. S. Cao *et al.*, Chromatin accessibility dynamics during chemical induction of pluripotency. *Cell Stem Cell* **22**, 529–542.e525 (2018).
8. H. Fu *et al.*, Dynamics of telomere rejuvenation during chemical induction to pluripotent stem cells. *Stem Cell Rep.* **11**, 70–87 (2018).
9. Y. Long, M. Wang, H. Gu, X. Xie, Bromodeoxyuridine promotes full-chemical induction of mouse pluripotent stem cells. *Cell Res.* **25**, 1171–1174 (2015).
10. W. Wang *et al.*, Inhibition of Syk promotes chemical reprogramming of fibroblasts via metabolic rewiring and H2 S production. *EMBO J.* **40**, e106771 (2021).
11. L. Yang *et al.*, Transient Dux expression facilitates nuclear transfer and induced pluripotent stem cell reprogramming. *EMBO Rep.* **21**, e50054 (2020).
12. C. Chronis *et al.*, Cooperative binding of transcription factors orchestrates reprogramming. *Cell* **168**, 442–459.e420 (2017).
13. A. S. Knaupp *et al.*, Transient and permanent reconfiguration of chromatin and transcription factor occupancy drive reprogramming. *Cell Stem Cell* **21**, 834–845.e836 (2017).
14. J. M. Polo *et al.*, A molecular roadmap of reprogramming somatic cells into iPS cells. *Cell* **151**, 1617–1632 (2012).
15. G. Schiebinger *et al.*, Optimal-transport analysis of single-cell gene expression identifies developmental trajectories in reprogramming. *Cell* **176**, 928–943.e922 (2019).
16. R. Stadhouders *et al.*, Transcription factors orchestrate dynamic interplay between genome topology and gene regulation during cell reprogramming. *Nat. Genet.* **50**, 238–249 (2018).
17. A. Zviran *et al.*, Deterministic somatic cell reprogramming involves continuous transcriptional changes governed by Myc and epigenetic-driven modules. *Cell Stem Cell* **24**, 328–341.e329 (2019).
18. R. M. Evans, D. J. Mangelsdorf, Nuclear receptors, RXR, and the big bang. *Cell* **157**, 255–266 (2014).
19. N. Cabezas-Wallscheid *et al.*, Vitamin A-retinoic acid signaling regulates hematopoietic stem cell dormancy. *Cell* **169**, 807–823.e819 (2017).
20. B. Nie *et al.*, Brown adipogenic reprogramming induced by a small molecule. *Cell Rep.* **18**, 624–635 (2017).

21. K. Schonberger *et al.*, Multilayer omics analysis reveals a non-classical retinoic acid signaling axis that regulates hematopoietic stem cell identity. *Cell Stem Cell* **29**, 131–148.e110 (2022).
22. S. Kujawski *et al.*, Calcineurin regulates coordinated outgrowth of zebrafish regenerating fins. *Dev. Cell* **28**, 573–587 (2014).
23. H. S. Kaya-Okur *et al.*, CUT&Tag for efficient epigenomic profiling of small samples and single cells. *Nat. Commun.* **10**, 1930 (2019).
24. J. Houseley, D. Tollervey, The many pathways of RNA degradation. *Cell* **136**, 763–776 (2009).
25. C. R. Alonso, A complex "mRNA degradation code" controls gene expression during animal development. *Trends Genet.* **28**, 78–88 (2012).
26. S. L. Wolin, L. E. Maquat, Cellular RNA surveillance in health and disease. *Science* **366**, 822–827 (2019).
27. D. Papadopoulos *et al.*, MYCN recruits the nuclear exosome complex to RNA polymerase II to prevent transcription-replication conflicts. *Mol. Cell* **82**, 159–176.e112 (2022).
28. D. J. Morton *et al.*, The RNA exosome and RNA exosome-linked disease. *RNA* **24**, 127–142 (2018).
29. D. S. Mistry, Y. Chen, G. L. Sen, Progenitor function in self-renewing human epidermis is maintained by the exosome. *Cell Stem Cell* **11**, 127–135 (2012).
30. E. Pefanis *et al.*, Noncoding RNA transcription targets AID to divergently transcribed loci in B cells. *Nature* **514**, 389–393 (2014).
31. E. Pefanis *et al.*, RNA exosome-regulated long non-coding RNA transcription controls super-enhancer activity. *Cell* **161**, 774–789 (2015).
32. L. Nair *et al.*, Mechanism of noncoding RNA-associated N(6)-methyladenosine recognition by an RNA processing complex during IgH DNA recombination. *Mol. Cell* **81**, 3949–3964.e3947 (2021).
33. C. Mehta, I. Fraga de Andrade, D. R. Matson, C. N. Dewey, E. H. Bresnick, RNA-regulatory exosome complex confers cellular survival to promote erythropoiesis. *Nucleic Acids Res.* **49**, 9007–9025 (2021).
34. P. A. Ulmke *et al.*, Post-transcriptional regulation by the exosome complex is required for cell survival and forebrain development via repression of P53 signaling. *Development* **148** (2021).
35. B. Laffleur *et al.*, RNA exosome drives early B cell development via noncoding RNA processing mechanisms. *Sci. Immunol.* **7**, eabn2738 (2022).
36. J. Liu *et al.*, YTHDF2/3 are required for somatic reprogramming through different RNA deadenylation pathways. *Cell Rep.* **32**, 108120 (2020).
37. B. Laffleur, U. Basu, Biology of RNA surveillance in development and disease. *Trends Cell Biol.* **29**, 428–445 (2019).
38. B. Herquel *et al.*, Trim24-repressed VL30 retrotransposons regulate gene expression by producing noncoding RNA. *Nat. Struct. Mol. Biol.* **20**, 339–346 (2013).
39. A. Avgustinova *et al.*, Repression of endogenous retroviruses prevents antiviral immune response and is required for mammary gland development. *Cell Stem Cell* **28**, 1790–1804.e1798 (2021).
40. S. M. Zhang *et al.*, KDM5B promotes immune evasion by recruiting SETDB1 to silence retroelements. *Nature* **598**, 682–687 (2021).
41. M. Kato, K. Takemoto, Y. Shinkai, A somatic role for the histone methyltransferase Setdb1 in endogenous retrovirus silencing. *Nat. Commun.* **9**, 1683 (2018).
42. W. Sheng *et al.*, LSD1 ablation stimulates anti-tumor immunity and enables checkpoint blockade. *Cell* **174**, 549–563.e519 (2018).
43. J. Lee *et al.*, Activation of innate immunity is required for efficient nuclear reprogramming. *Cell* **151**, 547–558 (2012).
44. A. Chiche *et al.*, Injury-induced senescence enables in vivo reprogramming in skeletal muscle. *Cell Stem Cell* **20**, 407–414.e404 (2017).
45. L. Mosteiro *et al.*, Tissue damage and senescence provide critical signals for cellular reprogramming in vivo. *Science* **354**, aaf4445 (2016).
46. J. Mathieu *et al.*, Hypoxia-inducible factors have distinct and stage-specific roles during reprogramming of human cells to pluripotency. *Cell Stem Cell* **14**, 592–605 (2014).
47. L. Guo *et al.*, Resolving cell fate decisions during somatic cell reprogramming by single-cell RNA-seq. *Mol. Cell* **73**, 815–829.e817 (2019).
48. Y. Jin *et al.*, Data for "CD3254-RXRα axis promotes chemical reprogramming via RNA exosome-mediated MMVL30 degradation and inflammation suppression". NCBI Gene Expression Omnibus. https://www.ncbi.nlm.nih.gov/geo/query/acc.cgi?acc=GSE208771. Deposited 21 July 2022.